JGR Planets

RESEARCH ARTICLE

10.1029/2025JE009075

Key Points:

- Previous mud reservoirs indicated by mud volcanoes served as potential subsurface habitable environments
- The source depths of mud volcanoes may have ranged from 530 to 1,800 m, with maintained temperatures exceeding 20°C
- We suggest a candidate landing site for Tianwen-3 with high scientific value and safe engineering condition

Supporting Information:

Supporting Information may be found in the online version of this article.

Correspondence to:

J. Huang,
junhuang@cug.edu.cn

Citation:

Wang, L., Huang, J., Xiao, X., & Xiao, L. (2025). Subsurface habitable environments revealed by mud volcanoes in Utopia Planitia on Mars and implications for China's Tianwen-3 mission. *Journal of Geophysical Research: Planets*, *130*, e2025JE009075. https://doi.org/10.1029/2025JE009075

Received 11 MAR 2025
Accepted 11 AUG 2025

Author Contributions:

Conceptualization: Jun Huang
Funding acquisition: Jun Huang
Methodology: Le Wang, Xiao Xiao
Software: Le Wang, Xiao Xiao
Supervision: Jun Huang
Visualization: Le Wang, Jun Huang, Xiao Xiao, Long Xiao
Writing – original draft: Le Wang
Writing – review & editing: Le Wang, Jun Huang, Long Xiao

Subsurface Habitable Environments Revealed by Mud Volcanoes in Utopia Planitia on Mars and Implications for China's Tianwen-3 Mission

Le Wang[1], Jun Huang[1], Xiao Xiao[1,2], and Long Xiao[1]

[1]State Key Laboratory of Geological Processes and Mineral Resources, Hubei Key Laboratory of Planetary Geology and Deep Space Exploration, School of Earth Sciences, China University of Geosciences, Wuhan, China, [2]Now at Institute of Geochemistry, Chinese Academy of Sciences, Guiyang, China

Abstract The Vastitas Borealis Formation (VBF) has been hypothesized to represent sedimentary remnants of ancient northern martian oceans. Widely distributed pitted cones across VBF are interpreted as most likely mud volcanoes, whose source regions might have hosted habitable environments. Assuming these features are mud volcanoes, we constrained the depths of previous potential mud reservoirs using a isostatic eruption model. The results show that the depths of mud reservoirs may have ranged from approximately 530 to 1,800 m, with maintained temperatures exceeding 20°C under high geothermal heat flux (45–60 mW/m^2). Materials from these regions are of high priority for future sample return missions, for example Tianwen-3, the Mars sample return mission of China, aiming to search for martian biosignatures. Combing geological analysis and engineering constraints, we propose a scientifically very promising landing site in Utopia Planitia for Tianwen-3 mission.

Plain Language Summary The northern lowlands of Mars are covered by a continuous geologic unit called Vastitas Borealis Formation (VBF), which has been proposed to be remnants of an ancient northern ocean. There are conical features across VBF, which have summit depressions, and are thought to be mud volcanoes. Based on this assumption, we estimate the depth of previous potential mud reservoirs using a mud volcano eruption model. The results suggest that mud reservoirs lie 530–1,800 m deep and could have stayed above 20°C due to Mars's previous high geothermal flux (45–60 mW/m^2). The mud reservoirs with liquid water and high temperature might have hosted ancient habitats. Therefore, these areas are a priority for future sample-return missions, like China's Tianwen-3, which aims to search for Martian life. Combining geological and engineering factors, we selected a high-value landing site in Utopia Planitia for Tianwen-3 mission.

1. Introduction

Martian northern lowlands with continuous smooth topography have been proposed to be covered by ancient oceans (Head et al., 1999; Parker et al., 1993; Wang & Huang, 2024). Presently, the Vastitas Borealis Formation (VBF), interpreted as the depositional product of Hesperian catastrophic floods (Baker & Milton, 1974; Fairén et al., 2003), is considered as plausible remnants of the ancient oceans (Ivanov et al., 2014; Kreslavsky & Head, 2002; Lucchitta et al., 1986; Salvatore & Christensen, 2014). The globally distributed lobate margins (Ivanov et al., 2017) and sedimentary rock like dielectric constant (Mouginot et al., 2012) support the marine deposition origin of VBF. Recently, the Zhurong rover conducted in situ investigation of VBF and discovered shallow marine sedimentary structures (Xiao et al., 2023) and subsurface flood deposit strata (Li et al., 2022), further supporting the oceanic formation mechanism of VBF.

Pitted cones, extensively distributed along the outer margins of VBF (Chen et al., 2024; Mills et al., 2024), with various origins, have been interpreted as rootless cones (Fagents et al., 2002; Greeley & Fagents, 2001), pyroclastic cones (Ghent et al., 2012; West, 1974), tuff cones (Brož & Hauber, 2013), and mud volcanoes (Ivanov et al., 2014; Komatsu et al., 2016; Oehler & Allen, 2010; Skinner & Mazzini, 2009; Skinner & Tanaka, 2007). Recent studies suggest that mud volcano is the most likely origin for pitted cones in the northern lowlands of Mars (Brož et al., 2023; Huang et al., 2022; Wang et al., 2023; Ye et al., 2021; Zhang et al., 2024), which indicates the past presence of subsurface mud reservoirs. Additionally, the pancake-like ejecta and potential mudflows in the central regions of Utopia and Acidalia Planitiae have been proposed to be related to the subsurface mud reservoirs (Cuřín et al., 2023; Ivanov et al., 2015). Although directly dating the potential mud volcanoes remains

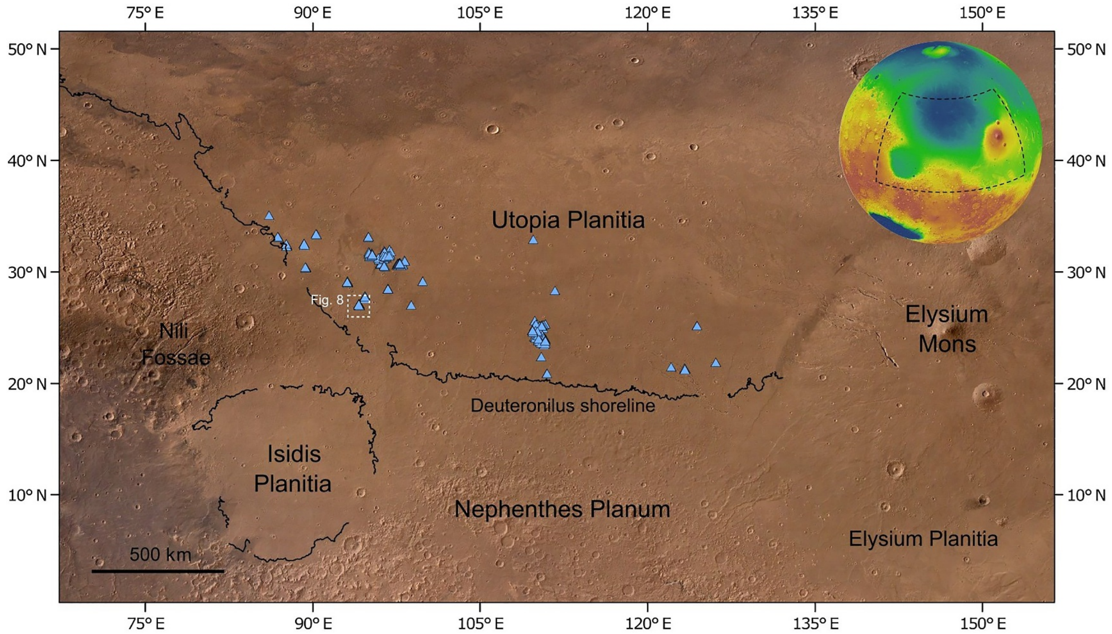

Figure 1. Geologic context of the study area. The blue triangles represent the identified pitted cones. Curved black lines indicate the margins of the VBF (Ivanov et al., 2017). The white dashed-line rectangle indicates the location of Figure 8. The base map is Tianwen-1 Moderate Resolution Imaging Camera (MoRIC) global mosaic (Liu et al., 2024) overlaying the Mars Orbiter Laser Altimeter (MOLA) shaded relief. The inset map shows the global location of Utopia Planitia, with the base map as the MOLA digital elevation model (DEM).

inaccessible, the ages of mudflows (3.46 Ga–544 Ma; Ivanov et al., 2014) and the surrounding VBF (3.6–3.0 Ga; (Ivanov et al., 2017; Tanaka et al., 2003)) suggest that the subsurface mud reservoirs in Utopia may have existed from the Late Hesperian to the Early Amazonian. In such a long period, there may have been a habitable environment hosting liquid water and moderate temperatures above freezing, which is beneficial to the survival of life. Therefore, we adopted the mud volcano origin for the pitted cones in Utopia Planitia to analyze the physical properties of potential mud reservoirs. Determining the depth of these mud reservoirs can help to constrain the habitable components in the mud reservoirs. Cluster and fractal analyses suggest that the source depth of pitted cones is approximately 7 km in Utopia Planitia (Zhang et al., 2024), and has three main ranges in Arcadia Planitia: 4–5, 14–23, and 50–55 km (De Toffoli et al., 2019, 2021). Thickness estimates for the VBF range from several hundred meters (Campbell et al., 2008; Head et al., 2002; Kreslavsky & Head, 2002), to 1–2 km (Buczkowski & Cooke, 2004), and up to 3 km (Cooke et al., 2011). This means that the pitted cones with source depth larger than 3 km may be fed by deeper fluids (mud or magma) underlying VBF. Here, we focus on estimating the depth of mud reservoirs in VBF through morphological analyses and numerical modeling of pitted cones in Utopia Planitia (Figure 1). In conjunction with the engineering constraints, we also discuss the landing site selection of Tianwen-3.

2. Materials and Methods

2.1. Data Materials

In the landing region of the Zhurong rover, we utilize digital image models (DIMs) from the High Resolution Camera (HiRIC, 0.7 m/pixel; Yan et al., 2021) onboard Tianwen-1 to identify pitted cones. Digital elevation models (DEMs, 3.5 m/pixel) derived from HiRIC data are employed to quantify the geometric parameters of these cones, with reported vertical and horizontal uncertainties of approximately 1 and 0.4 m, respectively (Yan et al., 2022). For regions within Utopia Planitia where HiRIC DEMs are unavailable, we analyze the morphological characteristics of pitted cones using images from the High Resolution Imaging Science Experiment (HiRISE, 0.25 m/pixel; McEwen et al., 2007) and DEMs generated from HiRISE stereo pairs through the Ames Stereo Pipeline (Beyer et al., 2018). We estimate the vertical error of HiRISE-derived DEMs by comparing them with the Mars Orbiter Laser Altimeter (MOLA) Precision Experiment Data Record (PEDR). We download the MOLA PEDR point shapefile data within the HiRISE DEM extent from the Mars Orbital Data Explorer. The

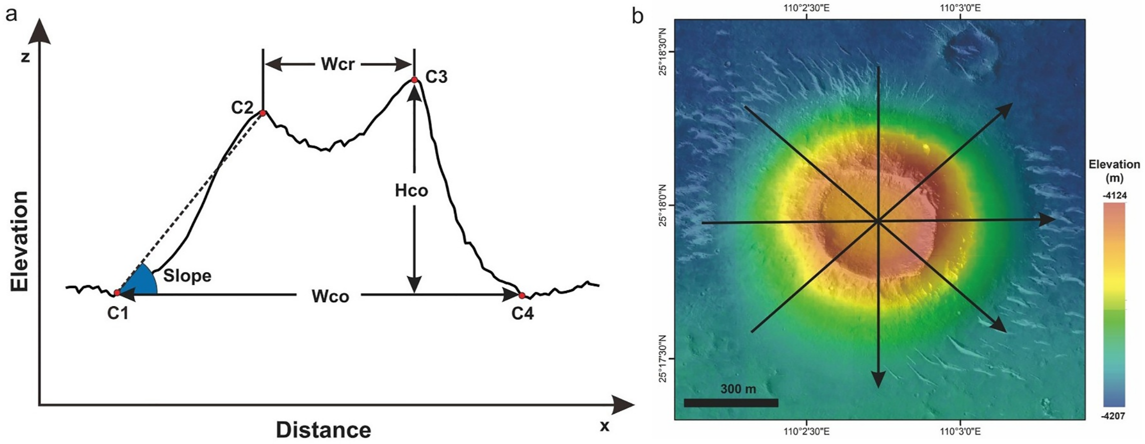

Figure 2. Diagram for the geometric parameters' measurement of potential mud volcanoes. (a) Geometric parameters for mud volcano, W_{cr} (diameter of summit pit), W_{co} (basal diameter), H_{co} (height) on a true topographic profile. Points C1–C4 are four control points for determining the boundaries. (b) Topographic profiles on the DEM.

average elevation difference between the MOLA and HiRISE DEMs at all MOLA PEDR points is used to estimate the vertical error of the HiRISE-derived DEMs, which is approximately 2 m. The dust cover index (DCI) map (16 pixel/degree; Ruff & Christensen, 2002), Thermal Inertia map (20 pixel/degree; Putzig et al., 2005) and rock abundance map (8 pixel/degree; Nowicki & Christensen, 2007) derived from Thermal Emission Spectrometer (TES) data are used to analyze the engineering conditions of a potential landing site of Tianwen-3 mission. A global database of pitted cones (Chen et al., 2024) was used to produce the density map.

2.2. Methods

We identified potential mud volcanoes within the study area using the high-resolution remote sensing images. Their geometric parameters were measured from the DEMs. By inputting these parameters into an isostatic eruption model—a framework simulating the eruptive processes of mud volcanoes—we estimated the thicknesses of overburden layers, corresponding to the burial depths of the potential mud reservoirs. Geothermal heating was then incorporated to further refine the estimated depths of the hypothesized mud reservoirs.

2.2.1. Geometric Parameters Measurement

The geometric parameters include summit pit diameters (W_{cr}), basal diameters (W_{co}), and the heights (H_{co}) of the mud volcanoes (Figure 2a). These parameters represent average values derived from four directional topographic profiles measured on the DEM (Figure 2b). For each direction, four control points (C1–C4) are defined along the profile (Figure 2a), corresponding to key inflection points in the topography. The summit pit diameter for each profile is defined as $x_{C3} - x_{C2}$, the basal diameter as $x_{C4} - x_{C1}$, and the cone height as $\max(z_{C2}, z_{C3}) - \min(z_{C1}, z_{C4})$. The three parameters, W_{cr}, W_{co}, and H_{co}, are necessary input values for the following numerical model. Therefore, we exclude the cones which cannot be used to measure these three indispensable geometric parameters. Because the model we used is an axisymmetric spreading model, the elliptic cones are also dropped to satisfy the calculation.

2.2.2. Isostatic Eruption Model

The isostatic eruption model assumes that buoyancy is the primary driving force for the eruption of potential mud volcanoes (Murton & Biggs, 2003). Under sufficient overburden pressure, a subsurface mixture of low-density, fine-grained sediments and liquid water becomes over-pressurized, and erupts to the surface (Kopf, 2002; Murton & Biggs, 2003). The mud volcano ceases to grow and reaches its maximum height when the overburden pressure equals that at the base of the mud conduit. The original height of a potential mud volcano, prior to erosion, can be used to estimate the burial depth of the associated mud reservoirs. The isostatic eruption model is composed of two processes: subsurface migration and surface spreading. We describe them in detail in the following sections.

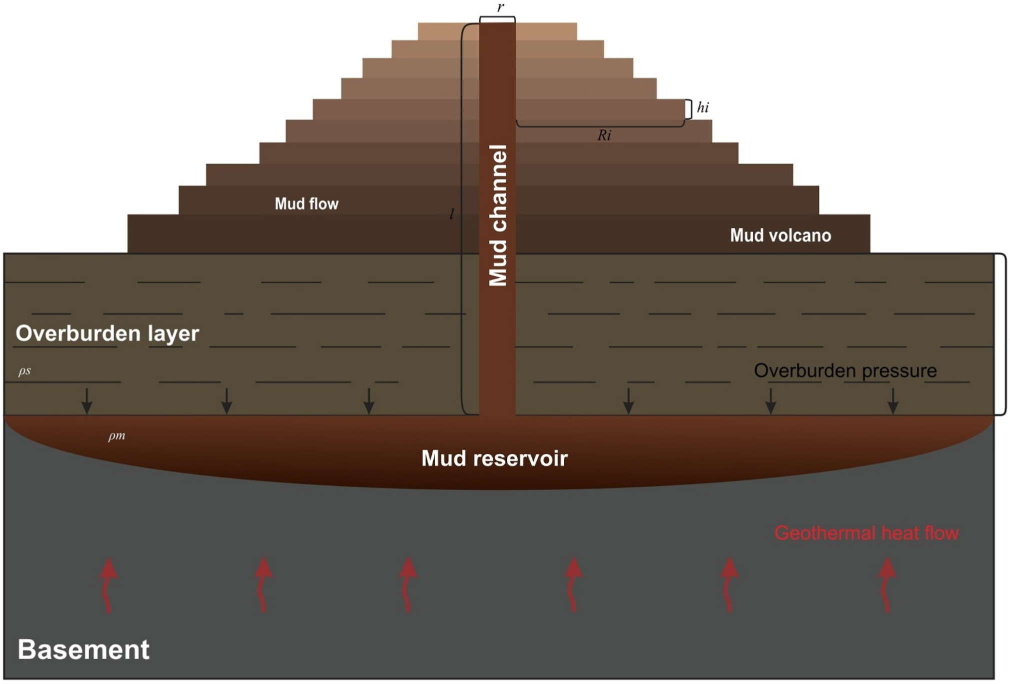

Figure 3. Sketch map of idealized mud volcano profile. The upper part illustrates the construction process of a mud volcano. R_i and h_i are the radius and thickness of mudflows, respectively. And r is the diameter of mud conduit. The lower parts represent the subsurface structure of a mud volcano, including the mud reservoir, overlying sediments, and mud conduit. Here, l is the length of mud conduit, ρ_s is the density of overburden, ρ_m is the density of mud, h_s is the burial depth of the potential mud reservoir.

2.2.2.1. *Thickness of Overburden Layers*

When the overburden pressure ($P_1 = h_s \rho_s g$) equals to the pressure at the base of the mud conduit ($P_2 = (h_s + H_{co}) \rho_m g$), we can obtain the burial depth of the potential mud reservoirs (Figure 3) h_s:

$$h_s = \frac{H_{co} \rho_m}{\rho_s - \rho_m} \tag{1}$$

where ρ_s and ρ_m are the densities of overburden layers and mud, respectively, g is the acceleration of gravity on Mars (3.71 ms^{-2}), H_{co} is the height of the potential mud volcanoes which is the lower limit value because of the possibility of erosion.

For the parameters in Equation 1, H_{co} is measured from DEMs, ρ_m and ρ_s depend on porosity and composition. The bulk density of mud ranges from 1,500 kg/m^3 for silty clays to 2,300 kg/m^3 for debris flow deposits (Kopf & Behrmann, 2000). Based on surface morphology of potential mud volcanoes, there are no obvious boulders, we assume ρ_m = 1,500, 1,800, and 2,000 kg/m^3. For overburden layers, two scenarios are considered: (a) dry sedimentary rocks, and (b) permafrost with ice-filled pores. The bulk density of overburden layers (ρ_s) is calculated as:

$$\rho_s = \phi \rho_f + (1 - \phi) \rho_g \tag{2}$$

where ϕ is porosity (0.25 or 0.45; De Bruin et al., 2021), ρ_f is the density of pore-filling materials (0.015 kg/m^3 for air (Petrosyan et al., 2011) or 920 kg/m^3 for water ice), and ρ_g is the grain density (2,900 or 3,100 kg/m^3; (Knapmeyer-Endrun et al., 2021; Wieczorek et al., 2022), i.e. the density of fully compacted crustal rocks). The resulting ρ_s ranges from 1,595 to 2,555 kg/m^3. Substituting the ρ_m and ρ_s into Equation 1 can get the burial depth h_s.

2.2.2.2. Subsurface Vertical Migration of Mud

The model of Newtonian fluid flow in a circular pipe (Turcotte & Schubert, 2014) is used to calculate the mud migration in conduit, with volumetric flow rate (Q) as:

$$Q = \frac{\Delta P \pi r^4}{8\mu l} \tag{3}$$

where ΔP is the pressure difference ($P_1 - P_2$), r is the conduit radius, μ is the mud dynamic viscosity, and l is the conduit length. The maximum r is assumed equal to the radius of summit pit ($W_{cr}/2$), though smaller radii (10%, 20%, 50%) are also tested due to the potential erosion.

The mud dynamic viscosity (μ) is estimated through an empirical equation (Hemmi & Miyamoto, 2018; Major & Pierson, 1992):

$$\mu = \alpha_2 \left(\frac{\tau_y}{\alpha_1}\right)^{\beta} \tag{4}$$

where α_1, α_2, β are constants ($\alpha_1 = 3.79 \times 10^{-6} Pa$; $\alpha_2 = 6.76 \times 10^{-17} Pa \cdot s$; $\beta = 2.23$) derived from the experimental analysis (Major & Pierson, 1992). The yield strength (τ_y) is:

$$\tau_y = \frac{\rho_m g H_{co}^2}{W_{co}} \tag{5}$$

The estimated μ ranges from 88 to 1.5×10^6 $Pa{\cdot}s$, consistent with terrestrial mudflows (Hemmi & Miyamoto, 2018; Kopf & Behrmann, 2000).

The eruption of mud is a continuous process. To simplify the calculation, we discretized the construction of a mud volcano into the successive emplacement of multiple separate mudflows (Figure 3). From Equation 3, we could get the flow rate for each mudflow as:

$$Q_i = \frac{\Delta P \pi r^4}{8 l_i \mu} \tag{6}$$

where i is the number of mudflow ($i = 0, 1, \ldots, n$), $l_i = (h_s + h_v)$ is the transient length of mud conduit, h_v ($\sum_{i=0}^{i=n} h_i$) is the transient height of mud volcano, h_i is the thickness of each mudflow (described below). The volumetric flow rate of each mudflow (Q_i) is a constant.

2.2.2.3. Surface Horizontal Spreading of Mudflow

The spreading of erupted mud is modeled using axisymmetric viscous flow theory (Didden & Maxworthy, 1982). In an ideal case, the erupted mudflows would extend radially outward, and form a pancake-like feature. We assume that the surface of each flow is horizontal, which indicates that the new mudflows are extruded in an identical way to their predecessors. Therefore, we consider the mudflow as thin cylinder, with radius of R_i and thickness of h_i (Figure 3) are given by:

$$h_i \approx \left(\frac{Q_i \nu_m}{g}\right)^{1/4} \tag{7}$$

$$R_i \approx \left(\frac{{Q_i}^3 g}{\nu_m}\right)^{1/8} {t_i}^{1/2} \tag{8}$$

where $\nu_m = (\mu_m/\rho_m)$ is kinematic viscosity, t is spreading time. The boundary condition is $R_0 = W_{co}/2$, and $h_0 = 0$. Substituting the flow rate of mudflow (Q_i) derived from Equation 6 into Equation 7, we could get the h_i. The only unknown variable in Equation 8 is flow time (t_i). The spreading time of the first mudflow (t_0) is:

$$t_0 = {R_0}^2 \left(\frac{{Q_0}^3 g}{\nu_m}\right)^{-1/4} \tag{9}$$

We assume the front velocity of each mudflow as a constant (U_0):

$$U_0 \approx \left(\frac{{Q_0}^3 g}{\nu_m}\right)^{1/8} {t_0}^{-1/2} \tag{10}$$

The spreading times of the next mudflows are:

$$t_i = \left(\frac{{Q_i}^3 g}{\nu_m}\right)^{1/4} \frac{1}{{U_0}^2} \tag{11}$$

Through iterating calculation of Q_i, R_i, and h_i until $\Delta P = 0$, we could derive the modeling profiles of the potential mud volcanoes.

2.2.3. Subsurface Temperature Calculation

The low temperature environment on Mars cannot sustain liquid water in the shallow subsurface. To further constrain the depth of the potential mud reservoirs, we calculated the geothermal temperature profile within the calculated depth range above. The subsurface temperature (T) is calculated using:

$$T = T_0 + \frac{q}{\lambda_s} h_s \tag{12}$$

where T_0 is the surface temperature, q is the surface heat flux, λ_s is the thermal conductivity of overburden layers, and h_s is the depth of potential mud reservoir. The surface temperature (T_0) is set at 235 K which is the maximum value derived from climate model in the period of 3.6 Ga–540 Ma (Wordsworth et al., 2021). The surface geothermal heat flux (q) is set as 15, 45, and 60 mW/m^2 (Broquet et al., 2020; Gyalay et al., 2020; Hauck & Phillips, 2002; Plesa et al., 2016; Ruiz, 2003) corresponding to the modeled values from present back to the Hesperian. The thermal conductivity of overburden layers (λ_s) is calculated as Ogawa et al. (2003):

$$\lambda_s = \phi \lambda_f + (1 - \phi) \lambda_g \tag{13}$$

where ϕ is the porosity, λ_f is the thermal conductivity of pore-filling materials, λ_g is the thermal conductivity of matrix.

The porosity of overburden layers (ϕ) is same as above, equal to 0.25, 0.45. The λ_f is 0.013 Wm^{-1}K^{-1} (Catalfamo et al., 2009) for air and 2.2 Wm^{-1}K^{-1} for water ice. We set λ_g as 1.5 or 2.0 Wm^{-1}K^{-1} (Gyalay et al., 2020). The thermal conductivities for overburden layers (λ_s) calculated by Equation 13 are 0.83, 1.11, 1.13, 1.50 Wm^{-1}K^{-1} for dry sedimentary rocks, and 1.82, 2.09, 1.68, 2.05 Wm^{-1}K^{-1} for permafrost. Consequently, the geothermal temperature profile is derived from Equation 12.

3. Result

3.1. Morphological Characteristics of Pitted Cones

The identified pitted cones (Figure 4a) are predominantly distributed along the southern margins of Utopia Planitia (Figure 1). It is necessary to measure the summit diameters of cones for calculating the mud flow rate in the isostatic eruption model. Consequently, cones lacking well-defined summit pits (Figure 4b) were excluded from the morphometric analysis. We measured the geometric parameters of the pitted cones. The results (Table S1

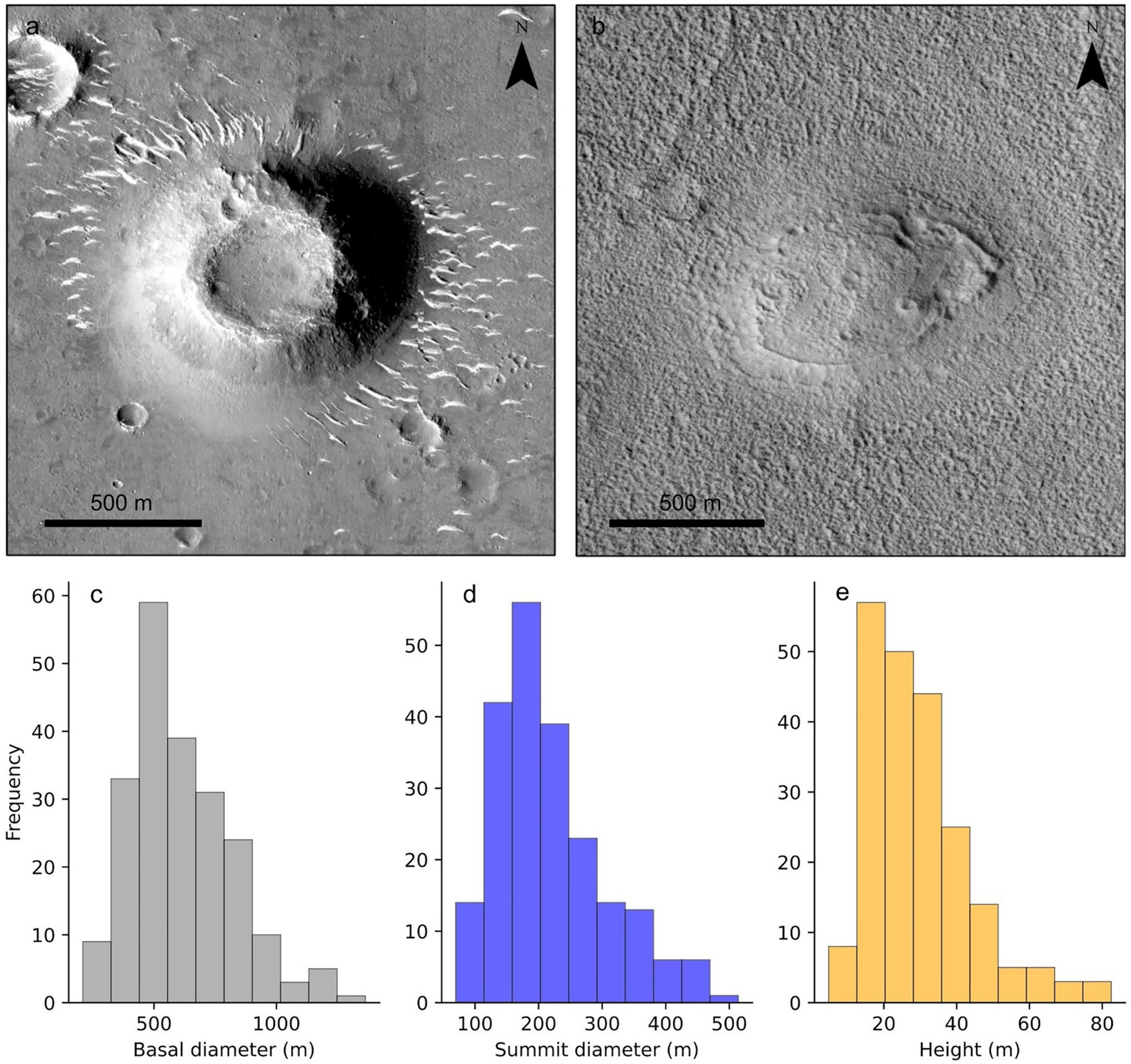

Figure 4. Morphological characteristics of pitted cones. (a) Pitted cone with a well-defined summit pit in the Zhurong landing region, centered at 109°51′24″E, 25°9′32″ N. HiRIC ID: HX1_GRAS_HIRIC_DIM_0.7_0004_251515N 1095850E_A. (b) Cone without summit pit, centered at 86°6′39″E, 35°0′30″N. HiRISE ID: ESP_047299_2155. (c–e). Histograms of mud volcano dimensions, including basal diameter, summit pit diameter, and height.

in Supporting Information S1) reveal that the heights of the mud volcanoes (H_{co}) range from approximately 5 to 80 m, with basal diameters (W_{co}) ranging from approximately 210 to 1,360 m, and the summit pit diameters (W_{cr}) varying between approximately 70 and 514 m (Figures 4c–4e). These geometric parameters were subsequently incorporated into the isostatic eruption model to estimate the burial depth of the potential mud reservoirs.

3.2. Depth of Mud Reservoirs

3.2.1. Depth From the Isostatic Eruption Model

Using the isostatic eruption model, we first calculate the thickness of overburden layers (Equations 1–2) as the preliminary depth of the potential mud reservoirs (h_s; Figure 3). The results primarily depend on the densities of mud (ρ_m) and overburden layers (ρ_s). For ρm, we adopt typical values for mud on Earth (1,500, 1,800, and 2,000 kg/m^3; Kopf & Behrmann, 2000). The ρ_s is estimated based on the porosity (ϕ), and the densities of pore-filling materials (ρ_f) and matrix grains (ρ_g) (Equation 2). Assuming the overburden layers consist of permafrost, ϕ

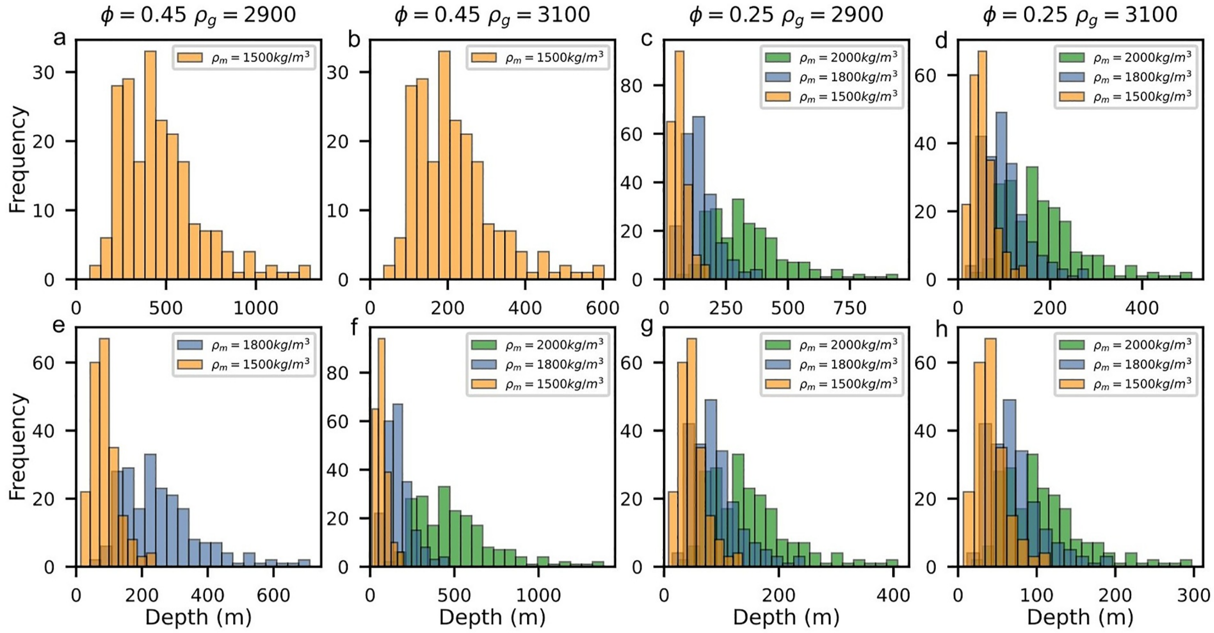

Figure 5. Frequency histogram for the calculated depths of potential mud reservoirs with different porosity of overburden layers (ϕ), and densities of mud (ρ_m) and matrix grains (ρ_g). (a–d). The overlaying strata is dry sedimentary rock. (e–h). The overburden layer is permafrost. The density of overburden layers (ρ_s) for panels (a–h) is 1,595, 1,705, 2,175, 2,325, 2,009, 2,119, 2,405, and 2,555 kg/m^3, respectively.

is set to 0.25 or 0.45 (ref. (De Bruin et al., 2021)), ρ_f is taken as 0.015 kg/m^3 for air (Petrosyan et al., 2011) or 920 kg/m^3 for water ice, and ρ_g is set to 2,900 or 3,100 kg/m^3 (Knapmeyer-Endrun et al., 2021; Wieczorek et al., 2022).

Using these parameter settings above, the estimated burial depth of the putative mud reservoirs (Figures 5a–5h) range from ∼7 m (ρ_m = 1,500 kg/m^3, ϕ = 0.25, ρ_s = 2,555 kg/m^3, Figure 5h) to ∼1,386 m (ρ_m = 2,000 kg/m^3, ϕ = 0.45, ρ_s = 2,119 kg/m^3, Figure 5f). Notably, when the density of the overburden layers is lower than that of the mud, the calculated depths are negative, which is physically implausible. Consequently, cases where ρ_s equaled to 1,595 or 1,705 kg/m^3, and ρ_m equaled to 1,800 or 2,000 kg/m^3 were excluded from the analysis (Figures 5a and 5b). Additionally, anomalously high depths (up to tens of kilometers) were observed when ρ_m and ρ_s are 2,000 kg/m^3 and 2,009 kg/m^3, respectively (Figure 5e). These unrealistic results were attributed to the minimal density difference between the mud and overburden layers, and were excluded further.

In summary, the preliminary burial depths of the potential mud reservoirs in the study area are estimated to range from ∼7 to 1,386 m.

Subsequently, we substitute h_s values calculated above into the equations governing the subsurface vertical migration and horizontal spreading of mud (Equations 3–13) to model the topographic profiles of the potential mud volcanoes. The density of mud (ρ_m) and the diameters of the mud conduits (W_{cr}) are key parameters in the calculation (Equations 3–13), with ρm remaining consistent with the values used above. Since the original mud conduit diameter cannot be observed directly, we constrain it indirectly using the summit pit diameter (W_{cr}), setting the mud conduit diameter to 10%, 20%, and 50% of W_{cr}. The resulting modeled topographic profiles were then compared to the actual values derived from the DEM (Figures 6a–6f).

The results indicate that the summits of the modeled mud volcanoes, with mud conduit diameters set to 10% and 20% of W_{cr}, are too narrow to be consistent with the observed profiles (Figures 6a and 6b). The only exception is the case with a mud conduit diameter of 50% (Figure 6c). However, in this scenario, the modeled profiles deviate significantly from the measured values (Figure 6c). This discrepancy can be attributed to the fixed spreading diameter (W_{co}) of the initial mudflow laye. Consequently, a wider mud conduit would lead to a larger erupted mud volume, producing thicker mudflows (Equation 3–8). By increasing the calculated height of the potential mud volcanoes (H_{co}) by 30%, 20%, and 10% (Figures 6d–6f), the flanks of the modeled profiles could intersect with the

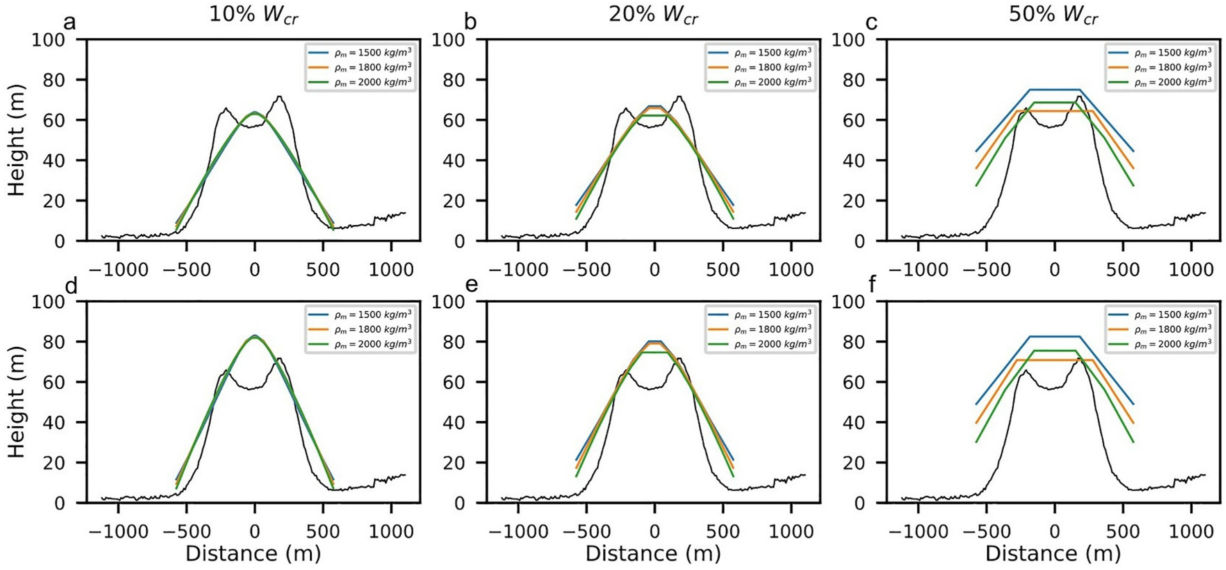

Figure 6. The modeled topographic profiles of a potential mud volcano centered at 25.651°N, 109.892°E. The graphs (a–c) are generated by using the original height of the potential mud volcano measured on the DEM. The graphs (d–f) are produced by increasing the modeled height of the pitted cones by 30%, 20%, and 10%. From left to right, the diameters of mud conduit for each column of graphs are set to 10%, 20%, and 50% of W_{cr}, respectively. The corresponding density of the overburden layers is 2,119 kg/m^3. The black line is the actual topographic profile measured from the HiRIC DEM.

margins of the summit pits of the observed profiles. This adjustment expands the estimated depth range of the potential mud reservoirs to approximately 8–1,802 m.

3.2.2. Depth Constrained by the Geothermal Heat Flux

The depth range of potential mud reservoirs (~8–1,802 m) estimated using the isostatic model is relatively broad. Given that stable liquid water cannot persist in the shallow subsurface under Mars' low ambient temperatures, we apply geothermal techniques to further constrain the depth. The critical parameters for calculating the geothermal temperature profiles include the surface heat flux (q), the thermal conductivity of overburden layers (λ_s), and the surface temperature (T_0) (Equation 12). For q, we adopted values of 15, 45, and 60 mW/m^2, corresponding to estimates for the Hesperian of Mars (Gyalay et al., 2020; Plesa et al., 2016; Ruiz, 2003). The λ_s is estimated based on the porosity (ϕ), as well as the thermal conductivities of pore-filling materials (λ_f) and matrix grains (λ_g) of the overburden layers. The maximum T_0 is set to 235 K, corresponding to the surface temperature in 3.6 Ga (Wordsworth et al., 2021). The results (Figures 7a–7h) indicate that ice does not melt within the depth range of potential mud reservoirs when q is set to 15 mW/m^2 (detailed melting cases in Table S2 in Supporting Information S1). However, when q increases to 60 mW/m^2, the shallowest melting depth is ~528 m (Figure 7a). Consequently, the depth of potential mud reservoirs, constrained by the geothermal gradient, is estimated to range from approximately 528 to 1,802 m.

4. Discussion

4.1. Origins for the Smaller Summit of the Modeled Mud Volcano

The summits of the modeled mud volcanoes, with mud conduit diameters set to 10% or 20% of W_{cr}, are smaller than the observed summit pits (Figures 6a and 6b). This discrepancy may result from erosion or collapse of the mud volcanic cone, leading to the enlargement of the summit pit over time. Indeed, when the height of the modeled profiles is increased by 20%–30%, the flanks intersect with the summit pit of the actual topographic profile (Figures 6d and 6e). Additionally, the eruptive style of the volcanoes could influence the shape of the volcanic cones. Here, we only consider the effusive eruption due to isostatic stress. Other driving stresses, such as excess pore fluid pressure (above hydrostatic), could cause explosive eruption. For a given basal diameter, more violent eruptions could produce a larger W_{cr}/W_{co} ratio (Wood, 1980), indicating that explosive eruption could also account for the larger summit pits observed in the actual topographic profiles.

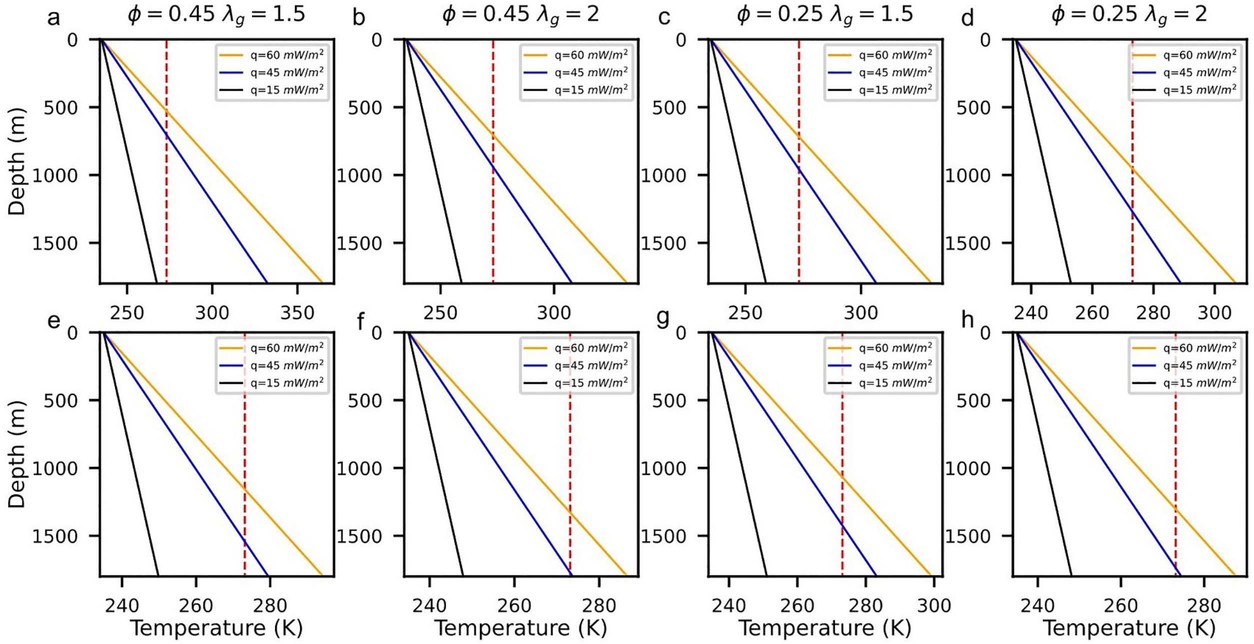

Figure 7. The subsurface temperature profile under different porosities (ϕ), matrix thermal conductivities (λ_g) of overburden layers. The constituent materials of the overburden layers are dry sediments (a–d), and permafrost (e–h). The thermal conductivities of the overburden layers for (a–h) are 0.83, 1.11, 1.13, 1.50, 1.82, 2.09, 1.68, and 2.05 $\mathrm{Wm^{-1}K^{-1}}$, respectively. The red dashed lines indicate a temperature equal to 273.15 K. The surface temperature (T_0) is 235 K.

4.2. Insights for Tianwen-3 Landing Site Selection

The Tianwen-3 (TW-3) mission is China's planned Mars sample return mission, with the primary scientific goal of searching for life signatures on Mars (Hou et al., 2024, 2025). The TW-3 mission's landing site selection is subject to several engineering constraints. These constraints include altitude limits of ≤–3 km, latitude ranges between 17° and 30°N, slopes ≤8°, and rock abundances ≤10% (Hou et al., 2024). Currently, Chryse and Utopia Planitiae are the favorable regions for the landing site selection (Hou et al., 2024). Based on the depth of mud reservoirs calculated above, combined with engineering constraints, we propose a potential landing site for the TW-3 mission (white ellipse in Figure 8). We adapt the dimension of Tianwen-1 landing ellipse 56 × 22 km (Wu et al., 2022). The selected landing ellipse is located in southwestern Utopia Planitia within the late Hesperian lowland unit (lHl; Tanaka et al., 2014). The ellipse satisfies the fundamental engineering constraints of TW-3, with specific parameters as follows: altitude <–3,600 m (Figure 8a), slope<2° (Figure 8b), rock abundance <10% (Figure 8c), and 95% of the area has a dust coverage index >0.95 (Figure 8d). The low dust covering rate is also indicated by the relatively high thermal inertia (Figure 8e). The sampling methods of TW-3 mission include surface scooping, subsurface drilling at a depth of 2 m, and mobile sampling with operational range >100 m (Hou et al., 2025). It is not plausible to have the spacecraft landed directly on the pitted cones, but the drone onboard TW-3 provides the possibility of collecting samples from potential mud volcanoes. We propose a potential landing ellipse for TW-3 with a relatively high density of mud volcanoes (Figure 8f) to make it more possible to acquire mud breccias ejected from the potential mud volcanoes.

On Earth, mud volcanoes are generally composed of evaporitic (e.g., gypsum, halite) and clay minerals (e.g., kaolinite, smectite, and vermiculite groups), which have low densities (Kopf, 2002). These low-density minerals record past water-related environments, such as river, lacustrine, or oceanic depositional settings. Clay minerals, in particular, are regarded as important indicators in the search for biosignatures on Mars (Hou et al., 2025). Although there is no spectral evidence of evaporitic or clay minerals in the potential mud volcanoes, the surrounding candidate oceanic remnants (VBF) could support the formation of clay-bearing sediments that feed such mud volcanoes. Therefore, samples from potential mud volcano fields hold high scientific value for TW-3 mission.

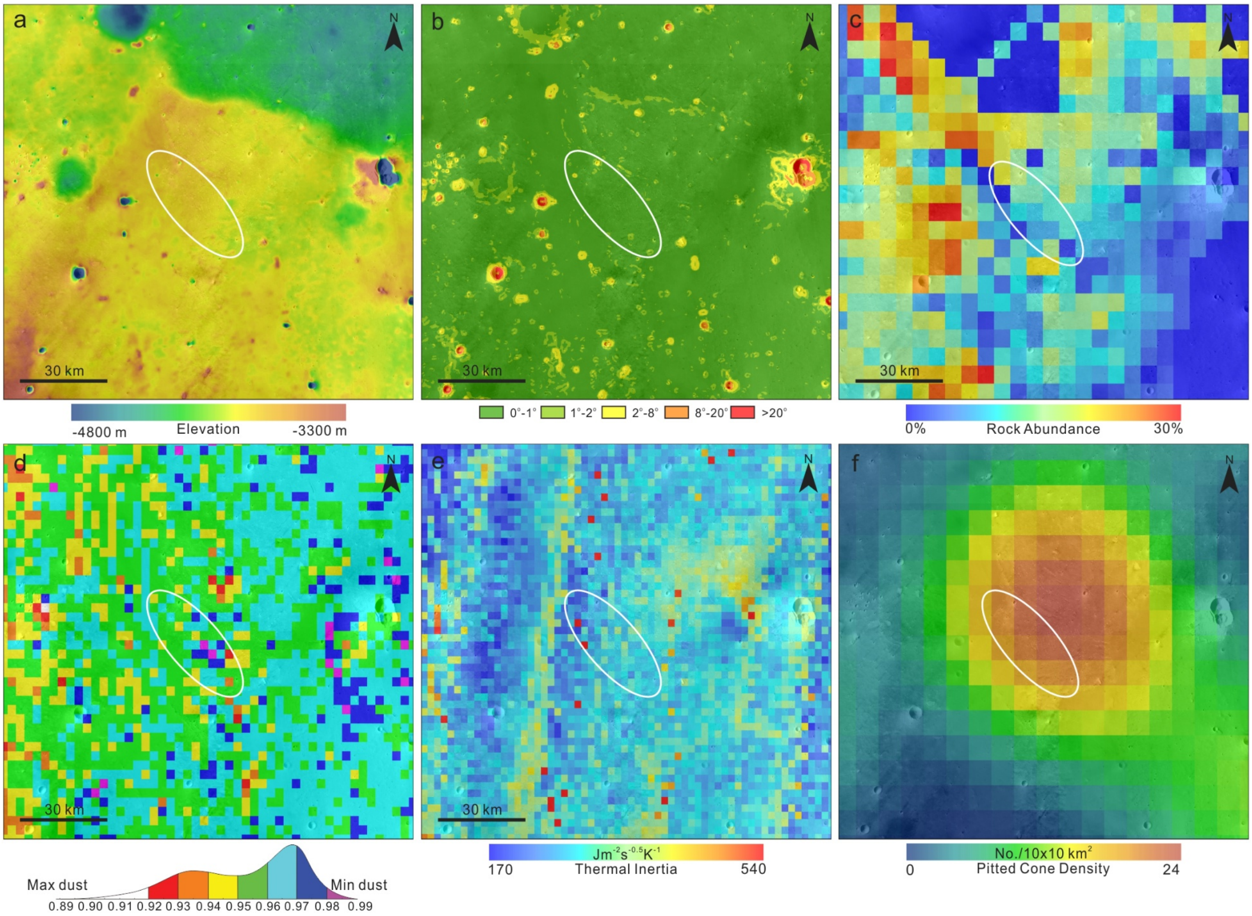

Figure 8. Engineering conditions of the potential landing site for Tianwen-3. (a) MOLA DEM shows that the elevation in the region is lower than −3,000 m. (b) Slope map derived from MOLA DEM. (c) TES Rock abundance map (Nowicki & Christensen, 2007). (d) TES Dust cover index (DCI) map (Ruff & Christensen, 2002). (e) TES thermal inertia map (Putzig et al., 2005). (f) Density map of pitted cones.

5. Conclusions

We estimate the source fluid depth of potential mud volcanoes in Utopia Planitia on Mars, suggesting previous potential mud reservoirs at depths of approximately 530–1,800 m. These mud reservoirs could have existed at temperatures of up to 20°C, supporting the presence of liquid water. Such habitable conditions are favorable for the potential survival of microbial life. Furthermore, the sediments within these mud reservoirs, interpreted as remnants of ancient oceans, may contain life signatures transported to the surface by mud volcanic eruptions and the excavations of impact craters. Consequently, these potential mud volcanoes and subsurface mud reservoirs hold significant scientific value for future in situ exploration and sample return missions, such as China's Tianwen-3.

Conflict of Interest

The authors declare no conflicts of interest relevant to this study.

Data Availability Statement

The Tianwen-1 data used in this study are available at https://moon.bao.ac.cn/web/enmanager/kxsj?missionName=HX1&zhName=HiRIC&grade=DIM-0.7 (DIMs), https://dx.doi.org/10.12350/CLPDS.GRAS.TW1.MoRIC-DOM_076_Global.vA (MoRIC global mosaic), and https://moon.bao.ac.cn/web/enmanager/kxsj?missionName=HX1&zhName=HiRIC&grade=DEM-3.5 (DEMs), and provided by China National Space Agency and the Science and Application Center for Moon and Deep Space Exploration. The HiRISE data used in this study are available in the NASA Planetary Data System (https://www.uahirise.org/). The MOLA DEM data used in this study is available at https://astrogeology.usgs.gov/search/map/mars_mgs_mola_dem_463m. The MOLA PEDR data is available at https://pds-geosciences.wustl.edu/missions/mgs/pedr.html. The MOLA shaded relief map is available at https://astrogeology.usgs.gov/search/map/mars_mgs_mola_global_shaded_relief_463m. The TES rock abundance and dust cover index data are available at http://www.mars.asu.edu/~ruff/DCI/dci.html. The TES thermal inertia map can be available at https://se.psi.edu/inertia/ti2003.html.

Acknowledgments

This work was supported by the National Natural Science Foundation of China (42441801). We appreciate the editorial handling by Editors Dr. Debra Buczkowski and Dr. Mike Sori. The reviews by Dr. Chris Okubo and Dr. Ernst Hauber greatly improved the manuscript. We thank Ms. Qiran Sa assistance in the measurements of some pitted cones.

References

Baker, V. R., & Milton, D. J. (1974). Erosion by catastrophic floods on Mars and Earth. *Icarus*, *23*(1), 27–41. https://doi.org/10.1016/0019-1035(74)90101-8

Beyer, R. A., Alexandrov, O., & McMichael, S. (2018). The Ames Stereo Pipeline: NASA's open source software for deriving and processing terrain data. *Earth and Space Science*, *5*(9), 537–548. https://doi.org/10.1029/2018EA000409

Broquet, A., Wieczorek, M. A., & Fa, W. (2020). Flexure of the lithosphere beneath the north polar cap of Mars: Implications for ice composition and heat flow. *Geophysical Research Letters*, *47*(5), e2019GL086746. https://doi.org/10.1029/2019GL086746

Brož, P., & Hauber, E. (2013). Hydrovolcanic tuff rings and cones as indicators for phreatomagmatic explosive eruptions on Mars. *Journal of Geophysical Research: Planets*, *118*(8), 1656–1675. https://doi.org/10.1002/jgre.20120

Brož, P., Oehler, D., Mazzini, A., Hauber, E., Komatsu, G., Etiope, G., & Cuřín, V. (2023). An overview of sedimentary volcanism on Mars. *Earth Surface Dynamics*, *11*(4), 633–661. https://doi.org/10.5194/esurf-11-633-2023

Buczkowski, D. L., & Cooke, M. L. (2004). Formation of double-ring circular grabens due to volumetric compaction over buried impact craters: Implications for thickness and nature of cover material in Utopia Planitia, Mars. *Journal of Geophysical Research*, *109*(E2), E02006. https://doi.org/10.1029/2003JE002144

Campbell, B., Carter, L., Phillips, R., Plaut, J., Putzig, N., Safaeinili, A., et al. (2008). SHARAD radar sounding of the Vastitas Borealis Formation in Amazonis Planitia. *Journal of Geophysical Research*, *113*(E12), E12010. https://doi.org/10.1029/2008JE003177

Catalfamo, C., Bruno, D., Colonna, G., Laricchiuta, A., & Capitelli, M. (2009). High temperature Mars atmosphere. Part II: Transport properties. *The European Physical Journal D*, *54*(3), 613–621. https://doi.org/10.1140/epjd/e2009-00193-6

Chen, Z., Wu, B., Krasilnikov, S., Xun, W., Ma, Y., Liu, S., & Li, Z. (2024). A global database of pitted cones on Mars for research on Martian volcanism. *Scientific Data*, *11*(1), 942. https://doi.org/10.1038/s41597-024-03811-1

Cooke, M., Islam, F., & McGill, G. (2011). Basement controls on the scale of giant polygons in Utopia Planitia, Mars. *Journal of Geophysical Research*, *116*(E9). https://doi.org/10.1029/2011JE003812

Cuřín, V., Brož, P., Hauber, E., & Markonis, Y. (2023). Mud flows in southwestern Utopia Planitia, Mars. *Icarus*, *389*, 115266. https://doi.org/10.1016/j.icarus.2022.115266

De Bruin, J. G. H., Bense, V. F., & Van Der Ploeg, M. J. (2021). Inferring permafrost active layer thermal properties from numerical model optimization. *Geophysical Research Letters*, *48*(16), e2021GL093306. https://doi.org/10.1029/2021GL093306

De Toffoli, B., Massironi, M., Mazzarini, F., & Bistacchi, A. (2021). Rheological and mechanical layering of the crust underneath thumbprint terrains in Arcadia Planitia, Mars. *Journal of Geophysical Research: Planets*, *126*(11), e2021JE007007. https://doi.org/10.1029/2021JE007007

De Toffoli, B., Pozzobon, R., Massironi, M., Mazzarini, F., Conway, S., & Cremonese, G. (2019). Surface expressions of subsurface sediment mobilization rooted into a gas hydrate-rich cryosphere on Mars. *Scientific Reports*, *9*(1), 8603. https://doi.org/10.1038/s41598-019-45057-7

Didden, N., & Maxworthy, T. (1982). The viscous spreading of plane and axisymmetric gravity currents. *Journal of Fluid Mechanics*, *121*, 27–42. https://doi.org/10.1017/S0022112082001785

Fagents, S. A., Lanagan, P., & Greeley, R. (2002). Rootless cones on Mars: A consequence of lava-ground ice interaction. *Geological Society, London, Special Publications*, *202*(1), 295–317. https://doi.org/10.1144/GSL.SP.2002.202.01.15

Fairén, A. G., Dohm, J. M., Baker, V. R., de Pablo, M. A., Ruiz, J., Ferris, J. C., & Anderson, R. C. (2003). Episodic flood inundations of the northern plains of Mars. *Icarus*, *165*(1), 53–67. https://doi.org/10.1016/S0019-1035(03)00144-1

Ghent, R. R., Anderson, S. W., & Pithawala, T. M. (2012). The formation of small cones in Isidis Planitia, Mars through mobilization of pyroclastic surge deposits. *Icarus*, *217*(1), 169–183. https://doi.org/10.1016/j.icarus.2011.10.018

Greeley, R., & Fagents, S. A. (2001). Icelandic pseudocraters as analogs to some volcanic cones on Mars. *Journal of Geophysical Research*, *106*(E9), 20527–20546. https://doi.org/10.1029/2000JE001378

Gyalay, S., Nimmo, F., Plesa, A., & Wieczorek, M. (2020). Constraints on thermal history of Mars from depth of pore closure below InSight. *Geophysical Research Letters*, *47*(16), e2020GL088653. https://doi.org/10.1029/2020GL088653

Hauck, S. A., & Phillips, R. J. (2002). Thermal and crustal evolution of Mars. *Journal of Geophysical Research*, *107*(E7). https://doi.org/10.1029/2001JE001801

Head, J. W., Hiesinger, H., Ivanov, M. A., Kreslavsky, M. A., Pratt, S., & Thomson, B. J. (1999). Possible ancient oceans on Mars: Evidence from Mars orbiter laser altimeter data. *Science*, *286*(5447), 2134–2137. https://doi.org/10.1126/science.286.5447.2134

Head, J. W., Kreslavsky, M. A., & Pratt, S. (2002). Northern lowlands of Mars: Evidence for widespread volcanic flooding and tectonic deformation in the Hesperian Period. *Journal of Geophysical Research*, *107*(E1), 3-1–3-29. https://doi.org/10.1029/2000JE001445

Hemmi, R., & Miyamoto, H. (2018). High-resolution topographic analyses of mounds in southern Acidalia Planitia, Mars: Implications for possible mud volcanism in submarine and subaerial environments. *Geosciences*, *8*(5), 152. https://doi.org/10.3390/geosciences8050152

Hou, Z., Liu, J., Pang, F., Wang, Y., Li, Y., Xu, M., et al. (2025). In search of signs of life on Mars with China's sample return mission Tianwen-3. *Nature Astronomy*, *9*(6), 783–792. https://doi.org/10.1038/s41550-025-02572-0

Hou, Z., Liu, J., Xu, Y., Pang, F., Wang, Y., Qin, L., et al. (2024). The search for life signatures on Mars by the Tianwen-3 Mars sample return mission. *National Science Review*, *11*(11), nwae313. https://doi.org/10.1093/nsr/nwae313

Huang, H., Liu, J., Wang, X., Chen, Y., Zhang, Q., Liu, D., et al. (2022). The analysis of cones within the Tianwen-1 landing area. *Remote Sensing*, *14*(11), 2590. https://doi.org/10.3390/rs14112590

Ivanov, M. A., Erkeling, G., Hiesinger, H., Bernhardt, H., & Reiss, D. (2017). Topography of the Deuteronilus contact on Mars: Evidence for an ancient water/mud ocean and long-wavelength topographic readjustments. *Planetary and Space Science*, *144*, 49–70. https://doi.org/10.1016/j.pss.2017.05.012

Ivanov, M. A., Hiesinger, H., Erkeling, G., & Reiss, D. (2014). Mud volcanism and morphology of impact craters in Utopia Planitia on Mars: Evidence for the ancient ocean. *Icarus*, *228*, 121–140. https://doi.org/10.1016/j.icarus.2013.09.018

Ivanov, M. A., Hiesinger, H., Erkeling, G., & Reiss, D. (2015). Evidence for large reservoirs of water/mud in Utopia and Acidalia Planitiae on Mars. *Icarus*, *248*, 383–391. https://doi.org/10.1016/j.icarus.2014.11.013

Knapmeyer-Endrun, B., Panning, M. P., Bissig, F., Joshi, R., Khan, A., Kim, D., et al. (2021). Thickness and structure of the Martian crust from InSight seismic data. *Science*, *373*(6553), 438–443. https://doi.org/10.1126/science.abf8966

Komatsu, G., Okubo, C. H., Wray, J. J., Ojha, L., Cardinale, M., Murana, A., et al. (2016). Small edifice features in Chryse Planitia, Mars: Assessment of a mud volcano hypothesis. *Icarus*, *268*, 56–75. https://doi.org/10.1016/j.icarus.2015.12.032

Kopf, A., & Behrmann, J. H. (2000). Extrusion dynamics of mud volcanoes on the Mediterranean Ridge accretionary complex. *Geological Society, London, Special Publications*, *174*(1), 169–204. https://doi.org/10.1144/GSL.SP.1999.174.01.10

Kopf, A. J. (2002). Significance of mud volcanism. *Reviews of Geophysics*, *40*(2), 2-1–2-52. https://doi.org/10.1029/2000RG000093

Kreslavsky, M. A., & Head, J. W. (2002). Fate of outflow channel effluents in the northern lowlands of Mars: The Vastitas Borealis Formation as a sublimation residue from frozen ponded bodies of water. *Journal of Geophysical Research*, *107*(E12), 4-1–4-25. https://doi.org/10.1029/2001JE001831

Li, C., Zheng, Y., Wang, X., Zhang, J., Wang, Y., Chen, L., et al. (2022). Layered subsurface in Utopia Basin of Mars revealed by Zhurong rover radar. *Nature*, *610*(7931), 308–312. https://doi.org/10.1038/s41586-022-05147-5

Liu, J., Ren, X., Yan, W., Chen, W., Zeng, X., Zhang, X., et al. (2024). A 76-m per pixel global color image dataset and map of Mars by Tianwen-1. *Science Bulletin*, *69*(14), 2183–2186. https://doi.org/10.1016/j.scib.2024.04.045

Lucchitta, B. K., Ferguson, H. M., & Summers, C. (1986). Sedimentary deposits in the Northern Lowland Plains, Mars. *Journal of Geophysical Research*, *91*(B13), E166–E174. https://doi.org/10.1029/JB091iB13p0E166

Major, J. J., & Pierson, T. C. (1992). Debris flow rheology: Experimental analysis of fine-grained slurries. *Water Resources Research*, *28*(3), 841–857. https://doi.org/10.1029/91WR02834

McEwen, A. S., Eliason, E. M., Bergstrom, J. W., Bridges, N. T., Hansen, C. J., Delamere, W. A., et al. (2007). Mars reconnaissance orbiter's high resolution imaging science experiment (HiRISE). *Journal of Geophysical Research*, *112*(E5), 2005JE002605. https://doi.org/10.1029/2005JE002605

Mills, M. M., Bickel, V. T., McEwen, A. S., & Valantinas, A. (2024). A global dataset of pitted cones on Mars. *Icarus*, *418*, 116145. https://doi.org/10.1016/j.icarus.2024.116145

Mouginot, J., Pommerol, A., Beck, P., Kofman, W., & Clifford, S. M. (2012). Dielectric map of the Martian northern hemisphere and the nature of plain filling materials. *Geophysical Research Letters*, *39*(2). https://doi.org/10.1029/2011GL050286

Murton, B. J., & Biggs, J. (2003). Numerical modelling of mud volcanoes and their flows using constraints from the Gulf of Cadiz. *Marine Geology*, *195*(1–4), 223–236. https://doi.org/10.1016/S0025-3227(02)00690-4

Nowicki, S. A., & Christensen, P. R. (2007). Rock abundance on Mars from the Thermal Emission Spectrometer. *Journal of Geophysical Research*, *112*(E5). https://doi.org/10.1029/2006JE002798

Oehler, D. Z., & Allen, C. C. (2010). Evidence for pervasive mud volcanism in Acidalia Planitia, Mars. *Icarus*, *208*(2), 636–657. https://doi.org/10.1016/j.icarus.2010.03.031

Ogawa, Y., Yamagishi, Y., & Kurita, K. (2003). Evaluation of melting process of the permafrost on Mars: Its implication for surface features. *Journal of Geophysical Research*, *108*(E4), 2002JE001886. https://doi.org/10.1029/2002JE001886

Parker, T. J., Gorsline, D. S., Saunders, R. S., Pieri, D. C., & Schneeberger, D. M. (1993). Coastal geomorphology of the Martian northern plains. *Journal of Geophysical Research*, *98*(E6), 11061–11078. https://doi.org/10.1029/93JE00618

Petrosyan, A., Galperin, B., Larsen, S. E., Lewis, S. R., Määttänen, A., Read, P. L., et al. (2011). The Martian atmospheric boundary layer. *Reviews of Geophysics*, *49*(3), RG3005. https://doi.org/10.1029/2010RG000351

Plesa, A.-C., Grott, M., Tosi, N., Breuer, D., Spohn, T., & Wieczorek, M. A. (2016). How large are present-day heat flux variations across the surface of Mars? *Journal of Geophysical Research: Planets*, *121*(12), 2386–2403. https://doi.org/10.1002/2016JE005126

Putzig, N. E., Mellon, M. T., Kretke, K. A., & Arvidson, R. E. (2005). Global thermal inertia and surface properties of Mars from the MGS mapping mission. *Icarus*, *173*(2), 325–341. https://doi.org/10.1016/j.icarus.2004.08.017

Ruff, S. W., & Christensen, P. R. (2002). Bright and dark regions on Mars: Particle size and mineralogical characteristics based on Thermal Emission Spectrometer data. *Journal of Geophysical Research*, *107*(E12), 2-1–2-22. https://doi.org/10.1029/2001JE001580

Ruiz, J. (2003). Amplitude of heat flow variations on Mars from possible shoreline topography. *Journal of Geophysical Research*, *108*(E11), 2003JE002084. https://doi.org/10.1029/2003JE002084

Salvatore, M. R., & Christensen, P. R. (2014). On the origin of the Vastitas Borealis Formation in Chryse and Acidalia Planitiae, Mars. *Journal of Geophysical Research: Planets*, *119*(12), 2437–2456. https://doi.org/10.1002/2014JE004682

Skinner, J. A., & Mazzini, A. (2009). Martian mud volcanism: Terrestrial analogs and implications for formational scenarios. *Marine and Petroleum Geology*, *26*(9), 1866–1878. https://doi.org/10.1016/j.marpetgeo.2009.02.006

Skinner, J. A., & Tanaka, K. L. (2007). Evidence for and implications of sedimentary diapirism and mud volcanism in the southern Utopia highland–lowland boundary plain, Mars. *Icarus*, *186*(1), 41–59. https://doi.org/10.1016/j.icarus.2006.08.013

Tanaka, K. L., Skinner, J. A., Dohm, J. M., Iii, R. P. I., Kolb, E. J., Fortezzo, C. M., et al. (2014). Geologic map of Mars. *Scientific Investigations Map. U.S. Geological Survey*. https://doi.org/10.3133/sim3292

Tanaka, K. L., Skinner, J. A. Jr., Hare, T. M., Joyal, T., & Wenker, A. (2003). Resurfacing history of the northern plains of Mars based on geologic mapping of Mars Global Surveyor data. *Journal of Geophysical Research*, *108*(E4). https://doi.org/10.1029/2002JE001908

Turcotte, D. L., & Schubert, G. (2014). Geodynamics. (3rd ed.). Cambridge University Press. https://doi.org/10.1017/CBO9780511843877

Wang, L., & Huang, J. (2024). Hypothesis of an ancient northern ocean on Mars and insights from the Zhurong rover. *Nature Astronomy*, *8*(10), 1220–1229. https://doi.org/10.1038/s41550-024-02343-3

Wang, L., Zhao, J., Huang, J., & Xiao, L. (2023). An explosive mud volcano origin for the pitted cones in southern Utopia Planitia, Mars. *Science China Earth Sciences*, *66*(9), 2045–2056. https://doi.org/10.1007/s11430-022-1119-1

West, M. (1974). Martian volcanism: Additional observations and evidence for pyroclastic activity. *Icarus*, *21*(1), 1–11. https://doi.org/10.1016/0019-1035(74)90085-2

Wieczorek, M. A., Broquet, A., McLennan, S. M., Rivoldini, A., Golombek, M., Antonangeli, D., et al. (2022). InSight constraints on the global character of the Martian crust. *Journal of Geophysical Research: Planets*, *127*(5), e2022JE007298. https://doi.org/10.1029/2022JE007298

Wood, C. A. (1980). Morphometric evolution of cinder cones. *Journal of Volcanology and Geothermal Research*, *7*(3), 387–413. https://doi.org/10.1016/0377-0273(80)90040-2

Wordsworth, R., Knoll, A. H., Hurowitz, J., Baum, M., Ehlmann, B. L., Head, J. W., & Steakley, K. (2021). A coupled model of episodic warming, oxidation and geochemical transitions on early Mars. *Nature Geoscience*, *14*(3), 127–132. https://doi.org/10.1038/s41561-021-00701-8

Wu, B., Dong, J., Wang, Y., Rao, W., Sun, Z., Li, Z., et al. (2022). Landing site selection and characterization of Tianwen-1 (Zhurong rover) on Mars. *Journal of Geophysical Research: Planets*, *127*(4), e2021JE007137. https://doi.org/10.1029/2021je007137

Xiao, L., Huang, J., Kusky, T., Head, J. W., Zhao, J., Wang, J., et al. (2023). Evidence for marine sedimentary rocks in Utopia Planitia: Zhurong rover observations. *National Science Review*, *10*(9), nwad137. https://doi.org/10.1093/nsr/nwad137

Yan, W., Liu, J., Ren, X., Li, C., Fu, Q., Wang, D., et al. (2021). Detection capability verification and performance Test for the high resolution imaging camera of China's Tianwen-1 Mission. *Space Science Reviews*, *217*(6), 71. https://doi.org/10.1007/s11214-021-00844-5

Yan, W., Ren, X., Liu, J., Zhang, L., Chen, W., Wang, D., et al. (2022). Topographic reconstruction of the "Tianwen-1" landing area on the Mars using high resolution imaging camera images. *IEEE Transactions on Geoscience and Remote Sensing*, *60*, 1–14. https://doi.org/10.1109/TGRS.2022.3206961

Ye, B., Qian, Y., Xiao, L., Michalski, J. R., Li, Y., Wu, B., & Qiao, L. (2021). Geomorphologic exploration targets at the Zhurong landing site in the southern Utopia Planitia of Mars. *Earth and Planetary Science Letters*, *576*, 117199. https://doi.org/10.1016/j.epsl.2021.117199

Zhang, J., Ren, X., Chen, Y., Zhang, H., Li, Z., Chen, Z., et al. (2024). Potential formational scenarios of the mud volcanoes in the Zhurong landing area in Utopia Planitia, observed by Tianwen-1. *Earth and Planetary Science Letters*, *647*, 119024. https://doi.org/10.1016/j.epsl.2024.119024